Journal of Applied Polymer Science

WILEY

Applied Polymer SCIENCE

RESEARCH ARTICLE OPEN ACCESS

Hydrophobic PVDF-Based Electrospun Nanofibrous Membranes: Design Criteria Fabrication and Resistance to Long-Term Hydrodynamic Operation

Félix Montero-Rocca | José David Badia-Valiente | Oscar Gil-Castell | Ramón Jiménez-Robles | Vicente Martínez-Soria | Marta Izquierdo

Research Group in Materials Technology and Sustainability (MATS), Department of Chemical Engineering, School of Engineering, University of Valencia, Burjassot, Spain

Correspondence: Marta Izquierdo (marta.izquierdo-sanchis@uv.es)

Received: 6 April 2025 | **Revised:** 10 June 2025 | **Accepted:** 22 June 2025

Funding: This work was supported by Ministerio de Ciencia e Innovacion (TED2021-131276A-I00) (PID2021-122495OA-I00) Conselleria d'Educacio, Investigacio, Cultura i Esport (CIACIF/2022/386) Ministerio de Universidades (FPU19/02478).

Keywords: degradation | electrospinning | membranes | separation techniques

ABSTRACT

The mechanical integrity of electrospun nanofiber membranes (ENMs) under operational conditions may limit their application in membrane contactors. This study integrated the electrospinning (ESP) with heat treatments to enhance nanofiber integrity in polyvinylidene fluoride (PVDF) ENMs. The impact of ESP parameters on the properties of the resulting ENMs was explored, including polymer dope flow rate (1.0–1.2 mL h^{-1}), tip-to-collector distance (TCD, 12–18 cm), and needle size (20–22 Ga), along with collector type (flat or rotary drum), needle motion (static or moving at 10 cm s^{-1}), and collector rotation speed were assessed. Heat treatment was evaluated at 130°C–170°C for 1–15 h. The optimized ENM exhibited a 134° ± 5° water contact angle, 200 ± 50 μm thickness, and 3.10 ± 0.02 mg cm^{-2} surface density. It was fabricated using a 1.20 mL h^{-1} polymer dope flow rate, 12 cm TCD, and a static 20 Ga needle during an 8-h ESP session with a rotary collector, followed by treatment at 150°C under 70 Pa for 6 h. It endured over 800 h under high hydraulic stress (21 L h^{-1} water flow), outperforming a commercial PVDF membrane and highlighting its potential for long-term operation in gas–liquid membrane contactor applications.

1 | Introduction

Membrane technologies can surpass conventional separation methods in chemical engineering, enabling tasks that are otherwise challenging. Membranes offer energy-efficient, compact, and selective solutions for various applications, including water purification [1, 2], food packaging [3], fuel cells [4–6], or biomedicine [7, 8], among others. In gas–liquid separation processes, membranes play a critical role in enabling efficient gas transfer in degassing [9–14] or gas absorption under harsh conditions [15, 16]. However, transferring their laboratory success to the industry scale demands

Abbreviations: A_M, Membrane sample area; A_θ, Degree of alignment (%); CH_4, Methane; d_F, Average nanofiber diameter; DMAc, Dimethylacetamide; DMF, Dimethylformamide; DMSO, Dimethylsulfoxide; ENM(s), Electrospun Nanofiber Membrane(s); ESP, Electrospinning; FESEM, Field emission scanning electron microscope; FSM, Flat-sheet module; m_{dry}, Mass of dry membrane sample; m_M, Membrane sample mass; m_{wet}, Mass of wet membrane sample; NMP, N-Methyl-2-pyrrolidone; N_T, Total number of sampled fibers; N_θ, Number of fibers with a given angle θ; PVDF, Polyvinylidene Fluoride; Q_{ESP}, Electrospinning dope flow rate; TCD, Tip-to-collector distance; T_{ESP}, Electrospinning fabrication time; T_{HT}, Heat treatment temperature; t_{HT}, Heat treatment time; TRL, Technology readiness level; V_{DOPE}, Electrospun dope volume (mL); WCA, Water contact angle; δ, Membrane thickness; ε, Porosity (%); ε_s, Membrane surface porosity; ρ_{C8OH}, n-Octanol density; σ, Membrane surface density (mg cm^{-2}).

significant advancements in fabrication techniques, material design, and scalability [17–19].

Membrane technology overcomes the drawbacks of conventional separation techniques like flooding, foaming, loading, and weeping. Instead, their long-term performance is affected by wetting and fouling, especially in applications involving highly contaminated or complex feeds [10, 11, 20, 21]. In aqueous environments, hydrophobic membranes are particularly effective in resisting the partial or complete occupation of the pores by the liquid, also known as pore wetting, due to their inherent water-repellent properties [22, 23]. These membranes preserve their structural integrity and performance by minimizing interactions with water molecules, ensuring their suitability for gas–liquid membrane contactors [14].

Traditional membrane fabrication methods, such as vapor-induced phase separation, nonsolvent-induced phase separation, track-etching, and sintering, involve manipulating polymer–solvent interactions, thermal processes, or chemical reactions to achieve the desired porosity, thickness, and surface characteristics [24, 25]. Selecting the proper technique is key to boosting desirable membrane properties. In this regard, electrospinning (ESP) emerged as a versatile and powerful technology that utilizes a high-voltage electric field to draw polymer solutions, producing nanofiber mats with specific and tunable structural properties, including high porosity and high surface area to volume ratio [26–28], with recent developments to boost ESP upscaling, such as centrifugal, roller, bubble, corona, and high-speed ESP [29]. These attributes make electrospun nanofiber membranes (ENMs) particularly attractive for applications requiring efficient separation, including freshwater production, desalination, or CO_2 capture by absorption [30–32]. Particularly, those made from polyvinylidene fluoride (PVDF) stand out due to their exceptional chemical resistance and hydrophobicity [33, 34].

Achieving a product with desirable properties through ESP requires balancing a complex interplay of parameters related to the solution, process, and environment [26, 35–38]. Solution parameters, such as polymer concentration, viscosity, and conductivity, dictate fiber formation and uniformity. Process parameters, including voltage, flow rate, and needle-to-collector distance, control the morphology and diameter of the fibers. Environmental factors like temperature and humidity influence solvent evaporation and fiber deposition. Imbalances between these factors lead to defects such as bead formation, inconsistent fiber diameters, or nonuniform mats [26, 35–38]. Therefore, optimizing these parameters in harmony is crucial to producing ENMs with the desired structural integrity, porosity, and functionality for specific applications.

The choice of nanofiber collector in the ESP equipment depends also on the desired properties and type of substrate. Flat collectors are commonly employed in applications requiring random fiber orientation [39], uniform fiber thickness [40], or when the study demands simplicity and versatility in membrane production [41]. Their ability to create isotropic mats makes them a baseline for comparative analyses and valuable for specific applications such as wound dressings [42] or scaffold production [43] in biomedical applications. Additionally, flat collectors are ideal for depositing thin films of randomly oriented fibers onto small-sized substrates [44]. On the other hand, rotary collectors are preferred for applications requiring mats with aligned fibers, as these exhibit higher crystallinity and enhanced mechanical resistance in a specific direction due to their anisotropic nature [45].

Regardless of the base material, untreated ENMs usually lack the required mechanical integrity to operate in their intended application [35, 46]. Among the most common postfabrication strategies to enhance the mechanical properties of ENMs, heat treatment or annealing stands out as one of the simplest and environmentally friendly approaches, since it only involves subjecting the polymer membrane to temperatures ranging from its glass-transition temperature to its melting point over a specific time without requiring more solvents or additives [35]. The membrane is typically placed between two plates to provide conductive heat, support, and flatness while facilitating handling, preventing adhesion, and ensuring uniform pressure distribution [47, 48].

The most commonly reported PVDF ESP conditions in the literature involve using a primary solvent, such as dimethylformamide (DMF), dimethylacetamide (DMAc), N-Methyl-2-pyrrolidone (NMP), or dimethylsulfoxide (DMSO), combined with acetone as a secondary solvent [49, 50]. Polymer concentrations range from 5 to 28 wt. %, the tip-to-collector distance (TCD) from 10 to 18 cm, and positive voltages from 8 to 35 kV [49, 51–53]. The resulting membranes exhibit WCAs between 115° and 146° [50, 52], average fiber diameters from 150 to 1300 nm [50, 51], and porosities ranging from 54% to 93% [51, 53]. These membrane properties are also influenced by the specific posttreatment process used.

This study aimed to evaluate the ESP and postprocessing conditions for fabricating hydrophobic flat-sheet PVDF ENMs with sufficient stability to endure prolonged hydraulic stress, serving as design criteria for gas–liquid separations in membrane contactors. The effects of key ESP parameters, including TCD, needle size, operating voltage, dope flow rate, and ESP time, were assessed to fabricate membranes suited for water treatment. The target properties included high hydrophobicity, thickness uniformity, and sufficient integrity for long-term service. Likewise, evaluating static and moving needle configurations, along with flat and rotary drum collectors, was highly relevant to determining the most suitable setup, with particular attention to the impact of rotation speed on membrane surface characteristics. Additionally, the influence of posttreatment consolidation temperature and time on membrane properties was examined, alongside stability tests in flat-sheet membrane contactors. Finally, benchmarking the ENMs with promising surface properties and resistance to hydraulic stress against a commercial membrane under simulated operational conditions provided relevant knowledge for the further operation of PVDF-based ENMs. This experimental approach aimed to improve the mechanical robustness and durability of the ENMs while preserving the unique properties essential for efficient operating performance.

2 | Materials and Methods

The study comprised three experimental sets: (1) fabrication of membranes through ESP by adjusting the parameters and setup to enhance the efficiency of the ENM fabrication process,

(2) evaluation of consolidation conditions to ensure membrane integrity, and (3) assessment of the stability of the fabricated ENMs under simulated operating conditions.

2.1 | Materials

The polymer powder, PVDF Kynar 761 (Mw ~440,000 g/mol [54]), was provided by Arkema (France). Dimethylformamide (DMF, 98% purity) and acetone (ACS grade) were purchased from VWR (USA). N-octanol (99% purity) was acquired from ThermoFisher Scientific.

2.2 | PVDF Membrane Fabrication by Electrospinning

The ESP dopes were prepared at a polymer concentration of 10 wt. % by dissolving PVDF powder in a 6:4 v/v % solution of DMF and acetone [49], in a Pyrex flask at 60°C and 175 rpm overnight in an orbital shaker (Rotaterm, J. P. Selecta, Barcelona, Spain). After homogenization, the solution was degassed for 24 h at room temperature and used for membrane preparation.

Nonwoven PVDF ENMs were produced in a Spinbox electrospinner (Bionicia, Paterna, Spain) in a horizontal setup by two different collectors: a 20 × 20 cm vertical stainless steel flat plate and an anodized aluminum rotary drum with a 10 cm diameter and a 20 cm length with 250 – 2000 rpm rotating speed. An aluminum foil layer covered the collectors for easy membrane detachment. A Sensirion SHT45-AD1B sensor (Sensirion, Stäfa, Switzerland) monitored the temperature and relative humidity inside the ESP chamber. During membrane fabrication, temperature was maintained within the range 24°C–26°C, and relative humidity was kept within the range 45%–55%. The electrospinner used two needle configurations: a needle with a scanning motion of 100 mm/s^{-1} (unidimensional and parallel to the collector), and a static needle. The tip-to-collector distance (TCD), needle size, dope flow rate (Q_{ESP}), and operating voltage were respectively adjusted from 12 to 18 cm, 20 to 22 Ga, 1.00 to 1.20 mL/h^{-1}, and 8 to 10 kV, to ensure a proper ESP process. Fabrication time (t_{ESP}) was selected from 1 to 10 h to adjust the resulting ENM thickness.

After production, the ENMs were dried overnight at 85°C in an oven (TCN 30 plus, Argolab, Carpi, Italy) to remove the residual solvent and stored for further consolidation under different heat treatment conditions.

2.3 | Heat Treatment Consolidation of Nanofibers

A heat treatment step was implemented to enhance fiber integrity in the membrane. ENM samples were placed between two glass plates and heated in an oven (TCN 30 plus, Argolab, Carpi, Italy) at a specified temperature and time, under an estimated applied pressure of 70 Pa. The membranes were preliminarily heat treated at 130°C for 15 h to provide an initial level of cohesion between fibers under mild conditions. Afterward, further heat treatment was applied at temperatures between 150°C and 170°C and times between 1 and 6 h.

2.4 | Membrane Characterization Techniques

ENMs were characterized based on membrane thickness and surface density, hydrophobicity, nanofiber morphology and alignment, overall porosity, and hydraulic stability under operational conditions.

The average membrane thickness (δ, μm) and its standard deviation were determined from 20 measurements with a low-force micrometer (543-705B Mitutoyo Digital Indicator ID-C, Mitutoyo, Japan).

The membrane surface density (σ, mg cm^{-2}), representing the average quantity of PVDF per unit membrane area, was determined using Equation (1), where m_M (mg) and A_M (cm^2) correspond to the sample's mass and area, respectively. Results were reported as the average and standard deviation of three samples. A laboratory scale (Denver Instrument SI-114, USA) measured the mass of the membrane samples.

$$\sigma = \frac{m_M}{A_M} \tag{1}$$

The hydrophobicity of the membranes was assessed using the sessile–drop water contact angle (WCA) measurement technique. A syringe pump (NE-300, KF Technology, Roma, Italy) dispensed water droplets on the membrane surface at five points. After a 15-s stabilization period, images of the droplets were captured using a digital microscope (Celestron Handheld Digital Microscope Pro, California, USA) with a white light source (Philips HUE Lamp, Amsterdam, The Netherlands) in the background. The images were analyzed with the Contact Angle plugin of ImageJ software, using the ellipse approximation method to calculate the WCA of at least five droplets per membrane, from which the average and its standard deviation were determined.

The surface morphology of the ENMs was examined using a Field Emission Scanning Electron Microscope (FESEM) (Hitachi S4800, Hitachi Ltd., Tokyo, Japan) at an accelerating voltage of 10 kV. Before imaging, the samples were coated with a thin layer of palladium–gold alloy using an SC7640 sputter-coater (1 min, 1.8 kV). The ImageJ software was used to determine the average fiber diameter (d_F, nm) and its standard deviation from 150 randomly selected fibers. The membrane surface porosity (ε_S) and its standard deviation were calculated from at least two SEM images at 2000× magnification [20].

The degree of alignment (A_θ, %) of the nanofibers was estimated with Equation (2), where N_θ represents the number of fibers with a given angle (θ), and N_T the total number of sampled fibers [55]. The orientation angle of around 180 randomly selected fibers was measured with the Image J software from SEM images.

$$A_\theta\,(\%) = \frac{N_\theta}{N_T} \bullet 100 \tag{2}$$

The overall membrane porosity was measured using a variation of the wet–dry method, with n-octanol as the wetting solvent.

Results were reported as an average and standard deviation from five membrane samples of 4 cm^2. The samples dehydrated in a laboratory oven at 60°C until they reached a constant weight (m_{dry}, mg). Each sample was then immersed in 10 mL of n-octanol inside 15 mL glass vials and subjected to 100 rpm orbital shaking at room temperature for 24 h. After full impregnation, the excess solvent was carefully removed and the wet samples were immediately weighed (m_{wet}, mg). The porosity (ε, %) was calculated using Equation (3), where ρ_{C8OH} represents the density of n-octanol (824 kg m^{-3} at 25°C), A_M (m^2) the sample area, and δ (m) the thickness.

$$\varepsilon\,(\%) = \frac{m_{wet} - m_{dry}}{\rho_{C8-OH} \bullet A_M \bullet \delta} \bullet 100 \quad (3)$$

2.5 | Membrane Integrity Test in Operation

The hydraulic stability of the membranes was assessed with a flat-sheet module (FSM, active area of 17.3 cm^2) by exposing them to a continuous distilled water flow rate of 21 L h^{-1} (liquid velocity of 16.8 cm s^{-1}), provided by a peristaltic pump (Percon N-M-II, JP Selecta, Barcelona, Spain), within a closed-loop system [9]. A scheme and a photograph of the experimental setup scheme are available in Figures 1 and S2. Membrane samples with a diameter of 6.5 cm were used. The test was extended until membrane failure or breakthrough, identified by water leakage on the module permeate side.

3 | Results and Discussion

The ESP parameters (TCD, needle size, voltage, and dope flow rate) were adjusted to obtain desirable membrane properties for efficient gas desorption from water streams in flat-sheet membrane contactors: high hydrophobicity and membrane integrity, assessed with the membrane breakthrough time under service conditions. Bulk properties, such as fiber arrangement, thickness, and surface density depend on the appropriate combination of the collector type, injection needle motion, and ESP time [26, 56, 57]. For the selection of the most suitable emitter–collector conditions, membranes were produced under the four possible combinations: (i) flat collector with a static needle, (ii) flat collector with moving needle, (iii) rotary drum collector with a static needle, and (iv) rotary drum collector with moving needle.

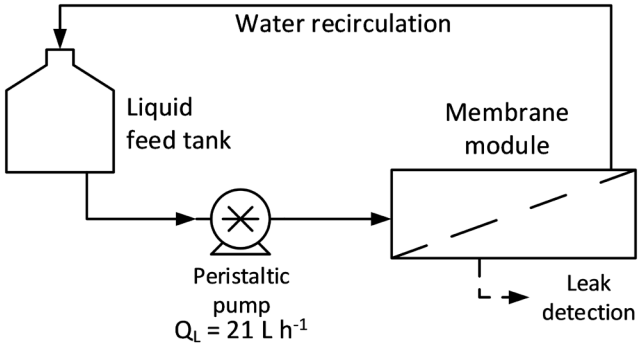

FIGURE 1 | Process flow diagram for hydraulic stability test.

3.1 | Steady PVDF Electrospinning Process in a Flat Collector and Static Needle

The initial attempts at ENM fabrication involved ≤3-h ESP sessions using a flat collector and a static needle. The TCD (12 and 18 cm), needle gauge (20 and 22 Ga), voltage (8.0 and 9.0 kV), and polymer flow rate (1.0 and 1.2 mL h^{-1}) were varied to obtain nanofibers, improve fiber collection efficiency, enhance thickness uniformity and membrane manipulability, and reduce the fabrication time for a target thickness. The resulting ESP fabrication conditions were a TCD of 12 cm, a needle gauge of 20 Ga, a voltage of 8.0 kV, and a dope flow rate of 1.20mL/h^{-1}. These conditions ensured effective solvent evaporation and a stable performance of Taylor's cone, without jet branching or splaying. Additionally, they prevented bead formation by maintaining a proper balance between surface tension and the electrical forces, which can be challenging in highly viscous solutions and under high electric fields [58]. The obtained ENMs were dried at 100°C for 1 h to promote the evaporation of the residual solvent, then subjected to glass-plate consolidation at 130°C overnight [50]. They showed high hydrophobicity (WCA around 128°), with an average thickness of 160 ± 20 μm, a surface density of 2.7 ± 0.1 mg/cm^{-2}, porosities in the 80%–90% range, and an average nanofiber diameter of 530 ± 160 nm. The experimental data related to the preliminary optimization of the ESP parameters are provided in (Table S1).

Further improvement of the fabrication of PVDF ENMs was explored by evaluating the effect of collector type, needle motion, speed of the rotary collector, and heat posttreatment.

3.2 | Effect of Collector Type and Needle Motion Regime on Membrane Morphology and Hydrophobicity

Membranes were produced using the four possible combinations of flat/rotary collector and static/moving needle to evaluate the impact of these parameters on membrane morphology and hydrophobicity. Figure 2a shows surface electron micrographs of the four resulting membranes, which exhibit a randomly aligned morphology of nonwoven nanofibers with the following average fiber diameters: 530 ± 160 and 390 ± 150 nm for the flat collector with static and moving needle, respectively, and 590 ± 170 and 450 ± 140 nm for the rotary collector with static and moving needle, respectively. Since all these samples consisted of fibers with diameters below 1000 nm, they qualify as ENMs. Also, the choice of collector type and needle motion appears to have no clear impact on fiber size, as all average fiber diameters fall within their respective uncertainty ranges, as shown in the fiber size histograms provided in the (Figure S3).This result is consistent with the findings of other authors [39].

Figure 2a also summarizes the results of these experiments in terms of WCA, thickness, and membrane surface density. Similar WCA values around 133° were obtained regardless of the collector type or needle motion. A maximum WCA difference of 5%, which fell well within the measurement uncertainty, was attributed to the inherent variability of the material. This result suggests that the collector type had no significant impact on membrane hydrophobicity, regardless of the needle movement regime.

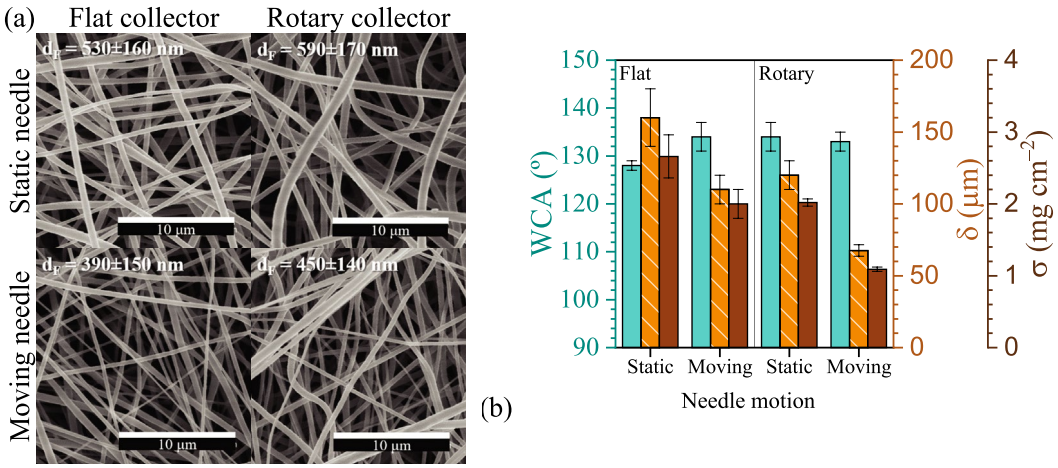

FIGURE 2 | (a) Surface electron micrographs and nanofiber diameter (d_F) of PVDF ENMs fabricated with flat or rotary collectors, and with static or moving needle. (b) Effect of needle motion and collector type in water contact angle (WCA,), thickness (δ,), and polymer surface density (σ,). ESP conditions: T_{ESP} = 2.5 h (flat collector); t_{ESP} = 5 h (rotary drum collector, 400 rpm); Q_{ESP} = 1.20 mL h^{-1}; TCD = 12 cm. Heat treatment: 130°C for 15 h. Bar errors represent the standard deviation. [Color figure can be viewed at wileyonlinelibrary.com]

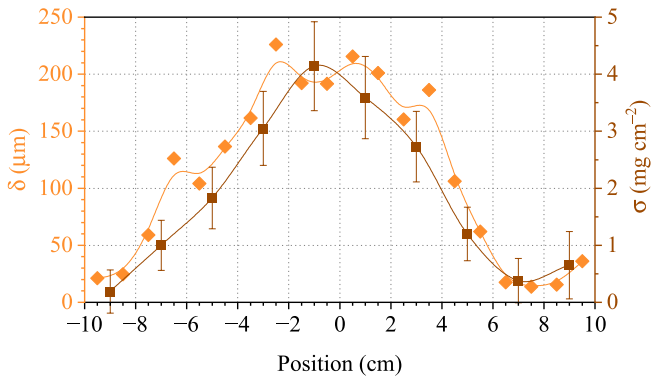

FIGURE 3 | Thickness (δ, ◆) and polymer surface density (σ, ■) profile for PVDF ENM. ESP conditions: Rotary drum collector at 400 rpm, static needle, Q_{ESP} = 1.20 mL h^{-1}, TCD = 12 cm, t_{ESP} = 8 h. Heat treatment: 130°C for 15 h. The 0 cm position corresponds to the central point of the collector. [Color figure can be viewed at wileyonlinelibrary.com]

Static-needle fabricated membranes exhibited higher thickness and polymer surface density than those produced with a moving needle, as anticipated. This was attributed to the static-needle setup directing fibers to a single point, typically the center of the collector, leading to increased thickness and polymer density in that area, as shown in Figure 3. Moreover, moving-needle fabricated membranes exhibited lower thickness standard deviations, regardless of the collector type, indicating greater thickness uniformity compared to those produced with a static needle. This aligns with the broader region of more evenly distributed fibers across the collector's breadth depicted in (Figure S4).

Membranes produced with the flat collector showed greater thickness and polymer surface density than those produced with the rotary collector, even though the latter operated for twice the duration (5 h vs. 2.5 h) to account for its 1.6 times larger collection area. These differences were attributed to the total available area on each collector, since the flat collector's smaller surface area allowed fibers to accumulate more densely, leading to faster thickness buildup. Ryu et al. reported that the thickness unevenness often found in electrospun mats was generated by the bending instabilities of the polymer jet, particularly affecting setups lacking the movement required to adjust the fiber nonuniform deposition [40], that is, those with a flat collector or static needle configuration used in this work.

Our results suggest that using a flat collector is a suitable choice when thickness and short-term production take priority over the total membrane area produced, such as during proof-of-concept testing. As shown in Figure 2b, rotary-collector ESP required a longer production time to achieve membrane thickness and surface densities comparable to those obtained with the flat collector, due to the wider distribution of fibers and greater collecting area. These results suggest that the rotary collector is better suited for scenarios requiring higher uniformity and membrane surface to meet quality standards. Consequently, to ensure uniform membranes while minimizing material waste and processing time, the rest of the study was conducted with the rotary collector and a moving needle.

3.3 | Effect of the Speed of the Rotary Collector on Fiber Morphology and Membrane Hydrophobicity

To achieve mechanically stable and isotropic membranes, a certain degree of entanglement provided by randomly oriented nonwoven fibers is desired. In contrast, highly aligned fibers would induce anisotropy, which is not desirable in this study. Rotary drum collector speeds between 400 and 900 rpm [59–61] were screened to assess their effect on fiber morphology and membrane hydrophobicity. Surface electron micrographs (Figure 4a) showed continuous, uniform, defect-free fibers with an apparently random orientation at all the rotary speeds studied. The average fiber diameter (d_F, around 470 nm) was unaffected by increasing collector speed from 400 to 900 rpm, unlike other studies reporting fiber diameter reduction due to greater and more sustained jet stretching forces at higher speeds [62–65].

Further analysis of the fiber alignment histograms (Figure 4b) revealed the influence of rotary speed on fiber alignment

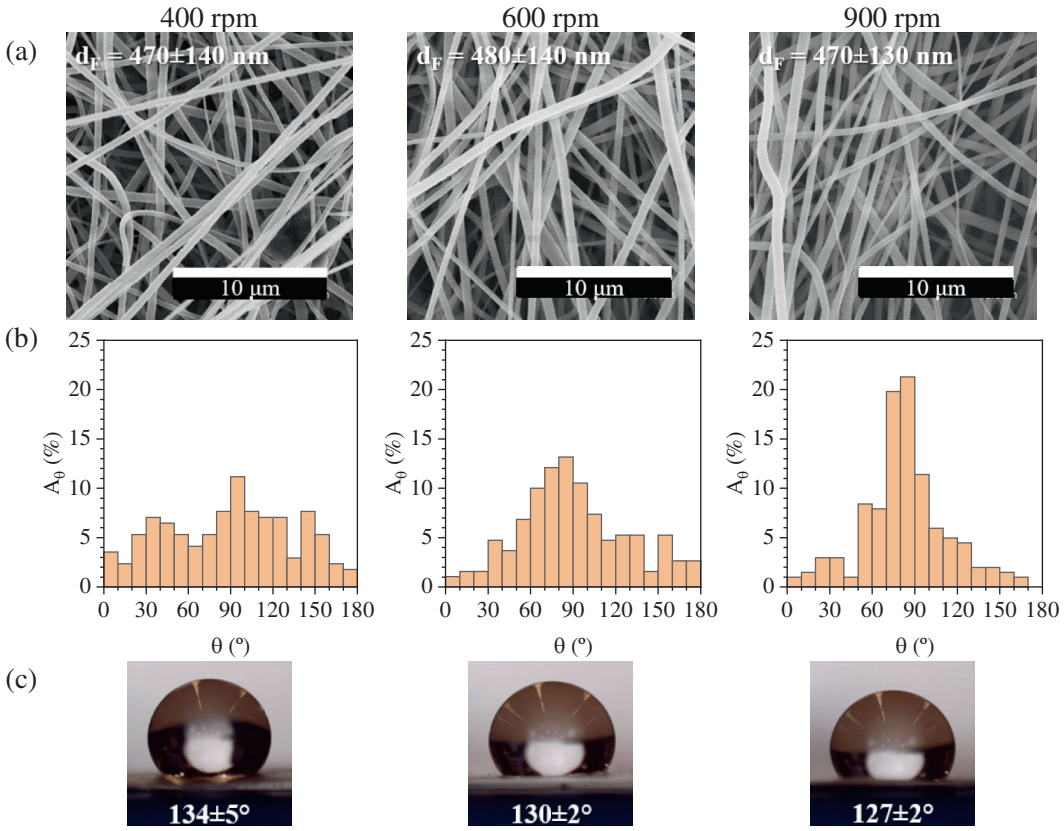

FIGURE 4 | (a) Surface electron micrographs and average nanofiber diameter (d_F), (b) fiber alignment degree (A_θ) vs. fiber angle (θ) histograms, and (c) water contact angle (WCA), of PVDF ENMs. ESP conditions: Rotary collector at 400, 600, and 900 rpm, moving needle, $Q_{ESP} = 1.10 mL/h^{-1}$. TCD = 12 cm. Heat treatment: 130°C for 15 h. [Color figure can be viewed at wileyonlinelibrary.com]

degree distribution in 10° interval bins. At 400 rpm, a broad distribution was evident, with all intervals showing alignment degrees below 12%. Similarly, other studies have reported membrane morphologies of randomly oriented fibers with alignment degrees around 10% for all intervals between 0° and 180° at a collector rotation speed of 300 rpm [66]. In our study, increasing the rotation speed to 600 rpm narrowed the alignment degree distribution to degree values between 10% and 15% for intervals within the 60°–100° range. As expected, at 900 rpm, the highest degree of alignment was observed, with values exceeding 20% for intervals between 70° and 90°. An alternative interpretation of these results involves evaluating the percentage of aligned fibers within a specific angle range. For fibers with angles between 80° and 100°, the percentages increased progressively with rotation speed, from 18% at 400 rpm to 24% at 600 rpm, and 33% at 900 rpm. Although higher rotation speeds improved the degree of alignment, the ENMs produced in this study cannot be classified as fully aligned. Achieving full alignment likely requires higher rotation speeds. For example, other researchers have reported 40% alignment at 85°–95° fiber with a rotation speed of 1000 rpm and over 90% alignment at 2000 rpm [55].

Additionally, lower rotary speed seems to slightly enhance membrane hydrophobicity (Figure 4c), with a maximum WCA of 134° ± 5° at 400 rpm and a minimum of 127° ± 2° at 900 rpm. So, a 400-rpm rotary speed was selected for subsequent membrane fabrication.

3.4 | Heat Treatment Effect on Fiber Morphology, Membrane Hydrophobicity, and Thickness

The preliminary exploration of heat treatment conditions focused on identifying suitable temperature and time ranges. Electrospun mats underwent changes in both bulk and surface properties following postfabrication heat-driven treatments (Figure 5), in line with expectations based on prior studies [50, 53].

The mats were first consistently subjected to heat treatment at 130°C and 70 Pa for 15 h as a first step, resulting in a surface morphology characterized by a network of randomly aligned nonwoven nanofibers, with no signs of sintering, indicating that the fibrous structure remained virtually unaltered. This strategy can be considered a preliminary strategy to enhance nanofiber cohesion under mild conditions, as suggested by other authors [50], who reported similar surface morphologies under comparable temperature and time conditions.

The mats were then subjected to a second heat treatment step involving more severe conditions, with temperatures of 150°C, 160°C, and 170°C, to further consolidate the nanofibers. Raising the treatment temperature to 150°C led to a slight increase in the number of fibers in the foreground while maintaining a predominantly nonsintered surface morphology, with only a few well-spaced sintered fibers, especially with prolonged times. At 160°C, sintered regions and fiber flattening became more evident with the formation of triangular junctions along the edges

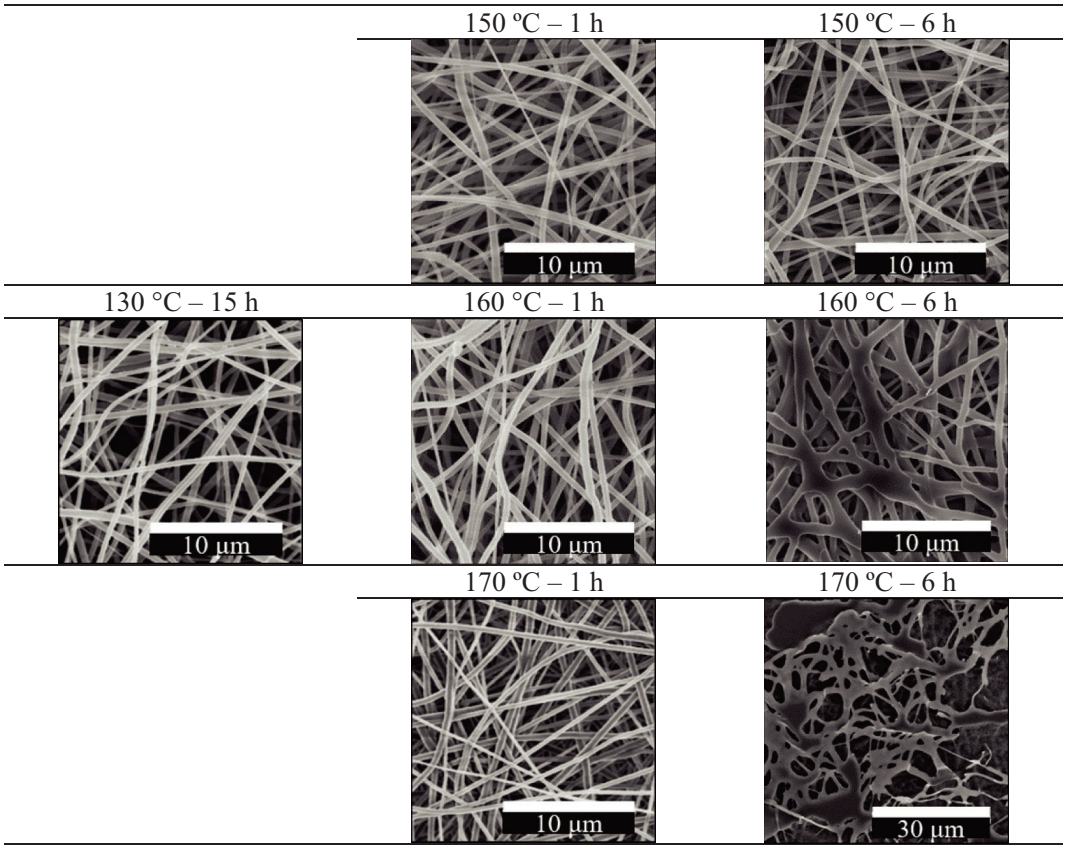

FIGURE 5 | Surface electron micrographs of PVDF electrospun nanofiber membranes heat-treated at different time and temperature conditions. ESP conditions: Rotary collector at 400 rpm, moving needle, $Q_{ESP} = 1.20\,mL/h^{-1}$, TCD = 12 cm, $t_{ESP} = 5\,h$.

of the fibers, particularly for treatment times of 6 h. Further increasing the temperature to 170°C caused PVDF to melt, destroying the fibrous structure as it approached its melting point. Other authors subjected PVDF ENMs to 1 h heat treatments at 170°C and 180°C. While the porous structure was preserved at both temperatures, severe sintering similar to our results at 160°C for 6 h was observed at 180°C [53]. This suggests that other factors such as the rate of heat transfer may also influence fiber morphology.

Given that 150°C and 160°C stood out as the most reasonable temperatures for achieving fiber compaction without compromising the nanofibrous morphology, a progressive evaluation was carried out at these temperatures with heat treatment times from 1 to 6 h. Figure 6a presents the effect of the heat-treatment temperature and time on membrane surface morphology. Because of these morphological modifications, heat treatment reduced the surface porosity at higher temperatures and longer durations (Figure 6b): from 13.2% ± 0.9% at 130°C for 15 h to a minimum of 7% ± 2% at 160°C for 6 h. This trend aligns with the greater number of fibers observed in the same focal plane under more intense heat-treatment conditions.

Figure 6b also illustrates the impact of the heat treatment temperature and time on membrane hydrophobicity and thickness. Membranes treated at 130°C for 15 h exhibited the highest WCA (134° ± 4°). A 10% WCA reduction was observed after additional 1-h treatments at 150°C and 160°C, while 6-h treatments led to a 13% reduction at 150°C and 17% at 160°C. The decline in hydrophobicity under more intense treatment conditions aligns with the observed membrane surface morphology. The mat treated at 130°C for 15 h consisted of nonwoven PVDF fibers loosely arranged due to electrostatic repulsion, likely exhibiting elevated roughness, which can enhance the natural tendency of a surface to repel or attract water [67]. Following a higher temperature heat treatment, however, fiber compression and potential sintering reduced roughness and, consequently, hydrophobicity.

In terms of membrane thickness, the second step of the heat treatment at 150°C preserved the average membrane thickness around 65 µm, while decreasing its variability, as indicated by a lower standard deviation. However, at 160°C, thickness decreased by 10% after 1 h and by 43% after 6 h, which is coherent with the surface porosity results. In summary, increasing the temperature and time of the heat treatment reduced membrane roughness, hydrophobicity, and thickness. Yao et al. observed similar results when heat-treating PVDF–HFP copolymers ENMs between flat metal plates at 140°C–170°C and 0.7–9.8 kPa for 1 to 8 h [68]. Liao et al. also described that higher heat-treatment temperatures within the 160°C–180°C range resulted in decreased hydrophobicity in their PVDF ENMs [53].

Based on the obtained results, an initial heat treatment at 130°C for 15 h followed by a second step at 150°C for 6 h, both under 70 Pa, was selected for further experiments, as it preserved the

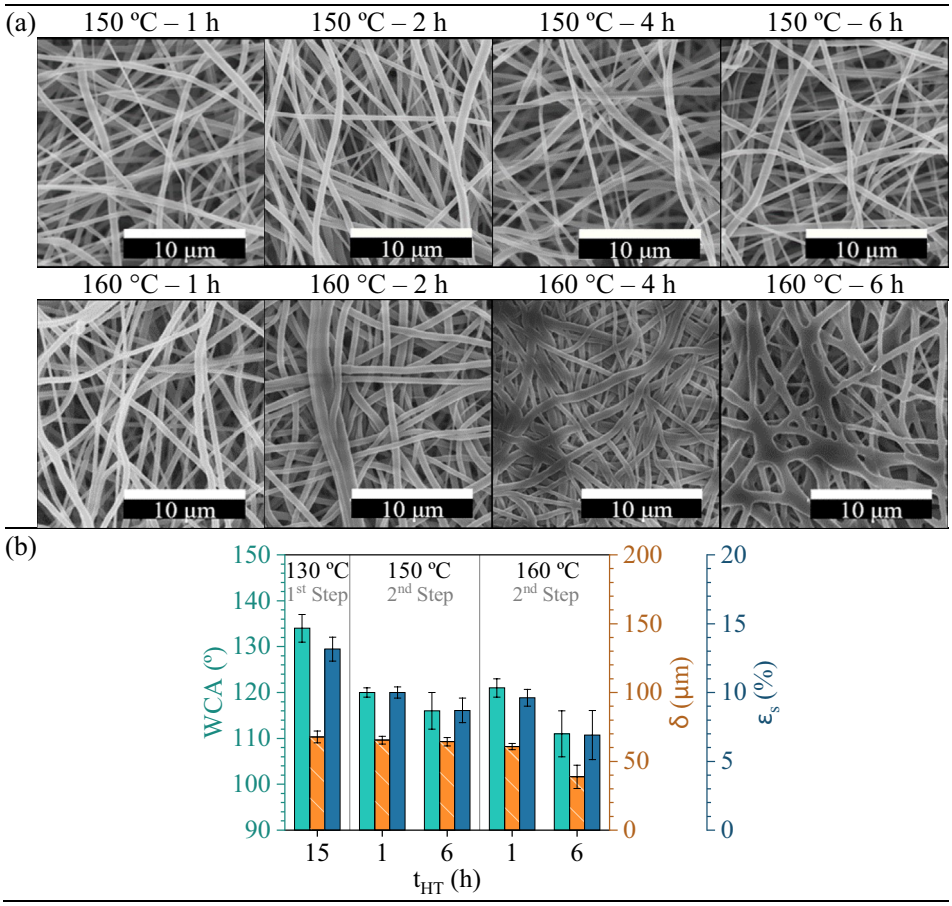

FIGURE 6 | Effect of the accumulative heat-treatment temperature (T_{HT}) and time (t_{HT}) on (a) membrane surface morphology and (b) water contact angle (WCA,), thickness (δ,), and surface porosity (ε_S,). ESP conditions: Rotary collector at 400 rpm, moving needle, $Q_{ESP} = 1.20\,mL\,h^{-1}$, TCD = 12 cm, $t_{ESP} = 5$ h. [Color figure can be viewed at wileyonlinelibrary.com]

nanofibrous structure while achieving membrane compaction without significantly compromising hydrophobicity.

3.5 | Membrane Integrity Under Simulated Hydraulic Operation

Although relatively rare in the literature, research on membrane stability under service conditions is essential for defining or forecasting the limiting operating parameters, useful lifetime, and long-term behavior of the membranes [9, 20, 69]. In this work, the membrane integrity test aimed to determine how long heat-treated membranes withstood simulated service conditions. ENMs were therefore subjected to a distilled water flow rate of 21 L h^{-1} in a flat-sheet module. This flow rate was specifically chosen based on our previous studies, which showed that higher rates caused structural damage to polymer-based membranes [9]. The experiments were extended until a water breakthrough was observed, and the breakthrough time was recorded.

Experiments with the previously presented membranes resulted in short breakthrough times (Figure 7a), which were attributed to their low thickness (< 70 µm) and polymer surface density (< 1.5 mg cm^{-2}), making them too thin for practical applications. Thus, to achieve thicker membranes, the ESP time was extended to 10 h while maintaining the previously established conditions. The results for these ENMs in terms of thickness and polymer surface density were interrelated, as both are extensive properties dependent on the amount of electrospun PVDF and the fiber collection method. A regression of these two parameters for the ENMs produced in this work (Figure 7b) suggested a linear relationship with an R^2 value close to 0.97. Surface density appeared to be a more reliable metric for determining the amount of polymer in the ENMs, as its measurement uncertainty is considerably lower than that of thickness measurements.

Figure 7a shows the hydraulic stability test results in a thickness versus breakthrough time plot, showing a clear relationship between both variables. Membranes with thicknesses between 110 and 120 µm (surface densities from 2.0 to 2.4 mg cm^{-2}) withstood 5 to 31 h of operation. Increasing thickness to 170 µm (surface density of 2.8 mg cm^{-2}) significantly enhanced hydraulic resistance, extending breakthrough time to 661 h. The thickest membrane, with around 200 µm and a surface density of 3.10 mg cm^{-2}, maintained its integrity for 839 h without failure, treating a total water volume of 17.6 m^3. At this point, the experiment was terminated, and the membrane kept its hydrophobicity (final WCA value around 135°), and its thickness was slightly reduced (final thickness 160 ± 20 µm), confirming the suitability for long-term operation. These results indicated that a minimum thickness of 170 µm and a polymer material surface density of 2.8 mg cm^{-2} were necessary for the breakthrough time to increase from less than 1 day

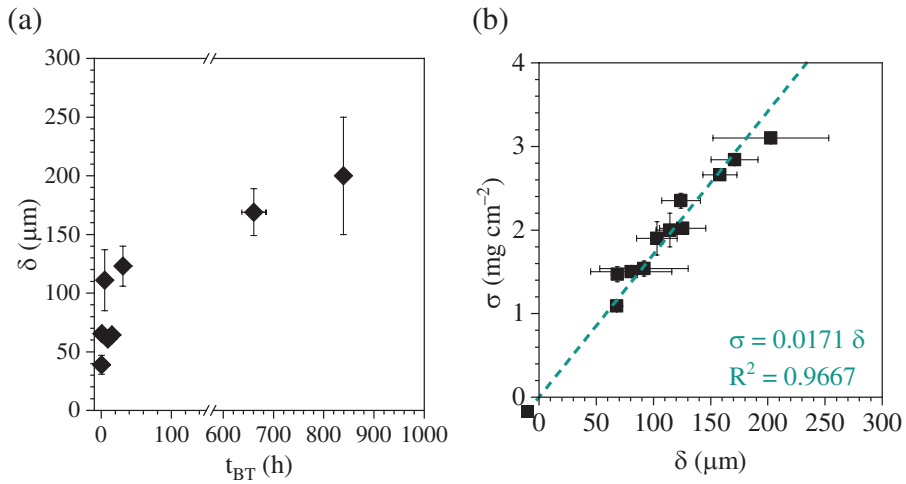

FIGURE 7 | (a) Membrane integrity under operation conditions: Membrane thickness (δ) vs. breakthrough time (t_{BT}); and (b) Polymer surface density (σ) vs. thickness (δ) for PVDF ENMs. ESP conditions: $Q_{ESP} = 1.20 mL/h^{-1}$. TCD = 12 cm. Heat treatment: 130°C for 15 h followed by 150°C for 6 h (70 Pa). [Color figure can be viewed at wileyonlinelibrary.com]

to beyond 25 days (600 h), for PVDF ENMs posttreated at 150°C for 6 h at 70 Pa. In other words, regardless of the collector type and needle movement regime, the membrane thickness and the surface density ultimately determined the hydraulic stability.

The ENMs of this work outperformed some commercial membranes under similar hydraulic stress conditions. For instance, commercial membranes of PDMS and PVDF were subjected to similar hydraulic stress conditions (21 L h^{-1} of water) in our previous work [9]. The PDMS membrane (overall thickness of 175 ± 5 μm) was tested for 95 h before breakthrough occurred (treated water volume of 2.0 m^3), which was attributed to the delamination of the dense layer. The PVDF membrane (159 ± 2 μm thickness) was used for 150 h (treated water volume: 3.2 m^3), with substantial structural changes at a microscopic level, attributed to plastic deformation induced by the hydraulic stress [9].

4 | Conclusion

The combination of the rotary drum collector and a moving needle was the most suitable configuration to increase the electrospinning yield while promoting homogeneous mats, reducing material waste, and minimizing the setup reconditioning time between electrospinning sessions.

The combined heat treatment with a first step at 130°C and 70 Pa for 15 h to improve the cohesion between the nanofibers under mild conditions, followed by a second and more severe step at 150°C in durations of 3–6 h maintained thickness and hydrophobic nature (WCA = 115°). These conditions, applied to 8 h electrospun ENMs, yielded thicknesses of around 200 μm and surface densities close to 3 mg cm^{-2}, and these ENMs exhibited excellent stability under a continuous water flux of 21 L h^{-1}, lasting over 800 h without failure, more than five times longer than a commercial PVDF membrane. In this regard, surface density was proposed as a complementary metric to thickness, with lower uncertainty, and strictly related to membrane long-term stability under service conditions. Therefore, PVDF ENMs have the potential for enduring service in membrane contactors for gas–liquid operation with aqueous feeds.

Author Contributions

Félix Montero-Rocca: conceptualization (supporting), data curation (lead), formal analysis (lead), investigation (lead), methodology (lead), validation (equal), visualization (lead), writing – original draft (lead), writing – review and editing (equal). **José David Badia-Valiente:** conceptualization (lead), funding acquisition (lead), methodology (equal), project administration (lead), supervision (supporting), validation (supporting), writing – review and editing (supporting). **Oscar Gil-Castell:** methodology (supporting), validation (supporting), writing – review and editing (supporting). **Ramón Jiménez-Robles:** methodology (supporting), validation (supporting), writing – review and editing (supporting). **Vicente Martínez-Soria:** conceptualization (supporting), funding acquisition (supporting), methodology (equal), project administration (supporting), supervision (lead), validation (equal), writing – review and editing (equal). **Marta Izquierdo:** conceptualization (lead), funding acquisition (lead), methodology (equal), project administration (lead), supervision (lead), validation (equal), writing – review and editing (equal).

Acknowledgments

This research is part of the projects TED2021-131276A-I00 and PID2021-122495OA-I00 funded by MCIN/AEI/10.13039/501100011033 and by the European Union NextGenerationEU/PRTR. F. Montero-Rocca's PhD grant was funded by the Generalitat Valenciana, Spain (CIACIF/2022/386). R. Jiménez-Robles' PhD grant was funded by Ministerio de Universidades, Spain (Beca de Formación de Profesorado Universitario FPU19/02478).

Conflicts of Interest

The authors declare no conflicts of interest.

Data Availability Statement

Data are available on ZENODO, https://doi.org/10.5281/zenodo.15622683

References

1. R. Zhang, Y. Liu, M. He, et al., "Antifouling Membranes for Sustainable Water Purification: Strategies and Mechanisms," *Chemical Society Reviews* 45 (2016): 5888–5924, https://doi.org/10.1039/c5cs00579e.

2. Z. Yang, Y. Zhou, Z. Feng, X. Rui, T. Zhang, and Z. Zhang, "A Review on Reverse Osmosis and Nanofiltration Membranes for Water

Purification," *Polymers* 11 (2019): 1252, https://doi.org/10.3390/polym11081252.

3. S. Torres-Giner, Y. Echegoyen, R. Teruel-Juanes, J. D. Badia, A. Ribes-Greus, and J. M. Lagaron, "Electrospun Poly(Ethylene-Co-Vinyl Alcohol)/graphene Nanoplatelets Composites of Interest in Intelligent Food Packaging Applications," *Nanomaterials* 8 (2018): 745, https://doi.org/10.3390/nano8100745.

4. O. Gil-Castell, Ó. Santiago, B. Pascual-Jose, E. Navarro, T. J. Leo, and A. Ribes-Greus, "Performance of Sulfonated Poly(Vinyl Alcohol)/graphene Oxide Polyelectrolytes for Direct Methanol Fuel Cells," *Energy Technology* 8 (2020): 2000124, https://doi.org/10.1002/ente.202000124.

5. R. Teruel-Juanes, C. del Río, O. Gil-Castell, C. Primaz, and A. Ribes-Greus, "Triblock SEBS/DVB Crosslinked and Sulfonated Membranes: Fuel Cell Performance and Conductivity," *Journal of Applied Polymer Science* 138 (2021): 50671, https://doi.org/10.1002/app.50671.

6. O. Gil-Castell, R. Teruel-Juanes, F. Arenga, et al., "Crosslinked Chitosan/Poly(Vinyl Alcohol)-based Polyelectrolytes for Proton Exchange Membranes," *Reactive and Functional Polymers* 142 (2019): 213–222, https://doi.org/10.1016/j.reactfunctpolym.2019.06.003.

7. O. Gil-Castell, I. Ontoria-Oviedo, J. D. Badia, E. Amaro-Prellezo, P. Sepúlveda, and A. Ribes-Greus, "Conductive Polycaprolactone/Gelatin/Polyaniline Nanofibres as Functional Scaffolds for Cardiac Tissue Regeneration," *Reactive and Functional Polymers* 170 (2022): 105064, https://doi.org/10.1016/j.reactfunctpolym.2021.105064.

8. O. Gil-Castell, J. D. Badia, I. Ontoria-Oviedo, D. Castellano, P. Sepúlveda, and A. Ribes-Greus, "Polycaprolactone/Gelatin-Based Scaffolds With Tailored Performance: *In Vitro* and *in Vivo* Validation," *Materials Science and Engineering: C* 107 (2020): 110296, https://doi.org/10.1016/j.msec.2019.110296.

9. R. Jiménez-Robles, C. Gabaldón, J. D. Badia, M. Izquierdo, and V. Martínez-Soria, "Recovery of Dissolved Methane Through a Flat Sheet Module With PDMS, PP, and PVDF Membranes," *Separation and Purification Technology* 282 (2022): 120057, https://doi.org/10.1016/J.SEPPUR.2021.120057.

10. R. Jiménez-Robles, V. Martínez-Soria, and M. Izquierdo, "Fouling Characterisation in PVDF Membrane Contactors for Dissolved Methane Recovery From Anaerobic Effluents: Effect of Surface Organofluorosilanisation," *Environmental Science and Pollution Research* 30 (2023): 29164–29179, https://doi.org/10.1007/s11356-022-24019-z.

11. M. Henares, P. Ferrero, P. San-Valero, V. Martínez-Soria, and M. Izquierdo, "Performance of a Polypropylene Membrane Contactor for the Recovery of Dissolved Methane From Anaerobic Effluents: Mass Transfer Evaluation, Long-Term Operation and Cleaning Strategies," *Journal of Membrane Science* 563 (2018): 926–937, https://doi.org/10.1016/j.memsci.2018.06.045.

12. J. Cookney, A. Mcleod, V. Mathioudakis, et al., "Dissolved Methane Recovery From Anaerobic Effluents Using Hollow Fibre Membrane Contactors," *Journal of Membrane Science* 502 (2016): 141–150, https://doi.org/10.1016/j.memsci.2015.12.037.

13. B. C. Crone, J. L. Garland, G. A. Sorial, and L. M. Vane, "Significance of Dissolved Methane in Effluents of Anaerobically Treated Low Strength Wastewater and Potential for Recovery as an Energy Product: A Review," *Water Research* 104 (2016): 520–531, https://doi.org/10.1016/j.watres.2016.08.019.

14. D. Hou, D. Jassby, R. Nerenberg, and Z. J. Ren, "Hydrophobic Gas Transfer Membranes for Wastewater Treatment and Resource Recovery," *Environmental Science & Technology* 53 (2019): 11618–11635, https://doi.org/10.1021/acs.est.9b00902.

15. L. Li, G. Ma, Z. Pan, N. Zhang, and Z. Zhang, "Research Progress in Gas Separation Using Hollow Fiber Membrane Contactors," *Membranes* 10 (2020): 380, https://doi.org/10.3390/membranes10120380.

16. S. Bavarella, A. Brookes, A. Moore, et al., "Chemically Reactive Membrane Crystallisation Reactor for CO2–NH3 Absorption and Ammonium Bicarbonate Crystallisation: Kinetics of Heterogeneous Crystal Growth," *Journal of Membrane Science* 599 (2020): 117682, https://doi.org/10.1016/j.memsci.2019.117682.

17. L. Francis, F. E. Ahmed, and N. Hilal, "Advances in Membrane Distillation Module Configurations," *Membranes* 12 (2022): 81, https://doi.org/10.3390/membranes12010081.

18. S. P. Nunes, P. Z. Culfaz-Emecen, G. Z. Ramon, et al., "Thinking the Future of Membranes: Perspectives for Advanced and New Membrane Materials and Manufacturing Processes," *Journal of Membrane Science* 598 (2020): 117761, https://doi.org/10.1016/j.memsci.2019.117761.

19. E. Drioli, F. Macedonio, and E. Tocci, "Membrane Science and Membrane Engineering for a Sustainable Industrial Development," *Separation and Purification Technology* 275 (2021): 119196, https://doi.org/10.1016/j.seppur.2021.119196.

20. R. Jiménez-Robles, M. Izquierdo, V. Martínez-Soria, L. Martí, A. Monleón, and J. D. Badia, "Stability of Superhydrophobicity and Structure of PVDF Membranes Treated by Vacuum Oxygen Plasma and Organofluorosilanisation," *Membranes* 13, no. 3 (2023): 314, https://doi.org/10.3390/MEMBRANES13030314.

21. Z. Wang and S. Lin, "Membrane Fouling and Wetting in Membrane Distillation and Their Mitigation by Novel Membranes With Special Wettability," *Water Research* 112 (2017): 38–47, https://doi.org/10.1016/j.watres.2017.01.022.

22. J. Kharaaz and A. An, "Patterned Superhydrophobic Polyvinylidene Fluoride (PVDF) Membranes for Membrane Distillation: Enhanced Flux With Improved Fouling and Wetting Resistance," *Journal of Membrane Science* 595 (2019): 117596, https://doi.org/10.1016/j.memsci.2019.117596.

23. M. R. Choudhury, N. Anwar, D. Jassby, and M. S. Rahaman, "Fouling and Wetting in the Membrane Distillation Driven Wastewater Reclamation Process – A Review," *Advances in Colloid and Interface Science* 269 (2019): 370–399, https://doi.org/10.1016/j.cis.2019.04.008.

24. B. S. Lalia, V. Kochkodan, R. Hashaikeh, and N. Hilal, "A Review on Membrane Fabrication: Structure, Properties and Performance Relationship," *Desalination* 326 (2013): 77–95, https://doi.org/10.1016/j.desal.2013.06.016.

25. X. Tan and D. Rodrigue, "A Review on Porous Polymeric Membrane Preparation. Part I: Production Techniques With Polysulfone and Poly (Vinylidene Fluoride)," *Polymers* 11 (2019): 1160, https://doi.org/10.3390/polym11071160.

26. Y. Li, J. Zhu, H. Cheng, et al., "Developments of Advanced Electrospinning Techniques: A Critical Review," *Advanced Materials Technologies* 6 (2021): 2100410, https://doi.org/10.1002/admt.202100410.

27. F. E. Ahmed, B. S. Lalia, and R. Hashaikeh, "A Review on Electrospinning for Membrane Fabrication: Challenges and Applications," *Desalination* 356 (2015): 15–30, https://doi.org/10.1016/J.DESAL.2014.09.033.

28. Y. Liao, C. H. Loh, M. Tian, R. Wang, and A. G. Fane, "Progress in Electrospun Polymeric Nanofibrous Membranes for Water Treatment: Fabrication, Modification and Applications," *Progress in Polymer Science* 77 (2018): 69–94, https://doi.org/10.1016/J.PROGPOLYMSCI.2017.10.003.

29. A. Keirouz, Z. Wang, V. S. Reddy, et al., "The History of Electrospinning: Past, Present, and Future Developments," *Advanced Materials Technologies* 8 (2023): 2201723, https://doi.org/10.1002/admt.202201723.

30. S. Santoro, I. Vidorreta, I. Coelhoso, et al., "Experimental Evaluation of the Thermal Polarization in Direct Contact Membrane Distillation Using Electrospun Nanofiber Membranes Doped With Molecular Probes," *Molecules* 24 (2019): 638, https://doi.org/10.3390/molecules24030638.

31. P. Yadav, R. Farnood, and V. Kumar, "Superhydrophobic Modification of Electrospun Nanofibrous Si@PVDF Membranes for

Desalination Application in Vacuum Membrane Distillation," *Chemosphere* 287 (2022): 132092, https://doi.org/10.1016/j.chemosphere.2021.132092.

32. G. Zainab, A. A. Babar, N. Iqbal, X. Wang, J. Yu, and B. Ding, "Amine-Impregnated Porous Nanofiber Membranes for CO2 Capture," *Composites Communications* 10 (2018): 45–51, https://doi.org/10.1016/j.coco.2018.06.005.

33. L. Deng, H. Ye, X. Li, et al., "Self-Roughened Omniphobic Coatings on Nanofibrous Membrane for Membrane Distillation," *Separation and Purification Technology* 206 (2018): 14–25, https://doi.org/10.1016/j.seppur.2018.05.035.

34. K. Li, D. Hou, C. Fu, K. Wang, and J. Wang, "Fabrication of PVDF Nanofibrous Hydrophobic Composite Membranes Reinforced With Fabric Substrates via Electrospinning for Membrane Distillation Desalination," *Journal of Environmental Sciences* 75 (2019): 277–288, https://doi.org/10.1016/j.jes.2018.04.002.

35. S. Nauman, G. Lubineau, and H. F. Alharbi, "Post Processing Strategies for the Enhancement of Mechanical Properties of ENMs (Electrospun Nanofibrous Membranes): A Review," *Membranes* 11 (2021): 39, https://doi.org/10.3390/membranes11010039.

36. J.-Y. Yin, C. Boaretti, A. Lorenzetti, A. Martucci, M. Roso, and M. Modesti, "Effects of Solvent and Electrospinning Parameters on the Morphology and Piezoelectric Properties of PVDF Nanofibrous Membrane," *Nanomaterials (Basel)* 12 (2022): 962, https://doi.org/10.3390/nano12060962.

37. C. J. Thompson, G. G. Chase, A. L. Yarin, and D. H. Reneker, "Effects of Parameters on Nanofiber Diameter Determined From Electrospinning Model," *Polymer* 48 (2007): 6913–6922, https://doi.org/10.1016/j.polymer.2007.09.017.

38. F. Topuz, M. A. Abdulhamid, T. Holtzl, and G. Szekely, "Nanofiber Engineering of Microporous Polyimides Through Electrospinning: Influence of Electrospinning Parameters and Salt Addition," *Materials & Design* 198 (2021): 109280, https://doi.org/10.1016/j.matdes.2020.109280.

39. D. Clavijo-Grimaldo, C. A. Casadiego-Torrado, J. Villalobos-Elías, A. Ocampo-Páramo, and M. Torres-Parada, "Characterization of Electrospun Poly(ε-Caprolactone) Nano/Micro Fibrous Membrane as Scaffolds in Tissue Engineering: Effects of the Type of Collector Used," *Membranes* 12 (2022): 563, https://doi.org/10.3390/membranes12060563.

40. H. I. Ryu, M. S. Koo, S. Kim, S. Kim, Y.-A. Park, and S. M. Park, "Uniform-Thickness Electrospun Nanofiber Mat Production System Based on Real-Time Thickness Measurement," *Scientific Reports* 10 (2020): 20847, https://doi.org/10.1038/s41598-020-77985-0.

41. Z. He, F. Rault, M. Lewandowski, E. Mohsenzadeh, and F. Salaün, "Electrospun PVDF Nanofibers for Piezoelectric Applications: A Review of the Influence of Electrospinning Parameters on the β Phase and Crystallinity Enhancement," *Polymers* 13 (2021): 174, https://doi.org/10.3390/polym13020174.

42. C. Gao, L. Zhang, J. Wang, et al., "Electrospun Nanofibers Promote Wound Healing: Theories, Techniques, and Perspectives," *Journal of Materials Chemistry B* 9 (2021): 3106–3130, https://doi.org/10.1039/D1TB00067E.

43. C. Vaquette and J. J. Cooper-White, "Increasing Electrospun Scaffold Pore Size With Tailored Collectors for Improved Cell Penetration," *Acta Biomaterialia* 7 (2011): 2544–2557, https://doi.org/10.1016/j.actbio.2011.02.036.

44. X. Wang, F. Sun, G. Yin, Y. Wang, B. Liu, and M. Dong, "Tactile-Sensing Based on Flexible PVDF Nanofibers via Electrospinning: A Review," *Sensors (Basel)* 18 (2018): 330, https://doi.org/10.3390/S18020330.

45. M. Bkkar, R. Olekhnovich, A. Kremleva, et al., "Influence of Electrospinning Setup Parameters on Properties of Polymer-Perovskite Nanofibers," *Polymers* 15 (2023): 731, https://doi.org/10.3390/polym15030731.

46. P. Sagitha, C. R. Reshmi, S. P. Sundaran, and A. Sujith, "Recent Advances in Post-Modification Strategies of Polymeric Electrospun Membranes," *European Polymer Journal* 105 (2018): 227–249, https://doi.org/10.1016/j.eurpolymj.2018.05.033.

47. M. Yao, Y. C. Woo, L. D. Tijing, C. Cesarini, and H. K. Shon, "Improving Nanofiber Membrane Characteristics and Membrane Distillation Performance of Heat-Pressed Membranes via Annealing Post-Treatment," *Applied Sciences* 7 (2017): 78, https://doi.org/10.3390/app7010078.

48. L. Li, R. Hashaikeh, and H. A. Arafat, "Development of Eco-Efficient Micro-Porous Membranes via Electrospinning and Annealing of Poly (Lactic Acid)," *Journal of Membrane Science* 436 (2013): 57–67, https://doi.org/10.1016/j.memsci.2013.02.037.

49. S. Gee, B. Johnson, and A. L. Smith, "Optimizing Electrospinning Parameters for Piezoelectric PVDF Nanofiber Membranes," *Journal of Membrane Science* 563 (2018): 804–812, https://doi.org/10.1016/J.MEMSCI.2018.06.050.

50. S. Santoro, I. M. Vidorreta, V. Sebastian, et al., "A Non-Invasive Optical Method for Mapping Temperature Polarization in Direct Contact Membrane Distillation," *Journal of Membrane Science* 536 (2017): 156–166, https://doi.org/10.1016/j.memsci.2017.05.001.

51. P. P. Putra, S. Akasaka, Y. Konosu, S. Zhang, A. Tanioka, and H. Matsumoto, "Structure–Piezoelectric Property Relationships of Thin Films Composed of Electrospun Aligned Poly (Vinylidene Fluoride) Nanofibers," *Nanomaterials (Basel)* 14 (2024): 491, https://doi.org/10.3390/nano14060491.

52. M. Pyo, K. H. Lee, and E.-J. Lee, "Enhancing Hydrophobicity Through Polydimethylsiloxane-Blended Poly(Vinylidene Fluoride-Co-Hexafluoropropylene) Electrospun Membranes: A Well-Designed Approach," *Polymer* 307 (2024): 127261, https://doi.org/10.1016/j.polymer.2024.127261.

53. Y. Liao, R. Wang, M. Tian, C. Qiu, and A. G. Fane, "Fabrication of Polyvinylidene Fluoride (PVDF) Nanofiber Membranes by Electro-Spinning for Direct Contact Membrane Distillation," *Journal of Membrane Science* 425 (2013): 30–39, https://doi.org/10.1016/J.MEMSCI.2012.09.023.

54. N. Padmavathy, P. K. Samantaray, L. D. Ghosh, G. Madras, and S. Bose, "Selective Cleavage of the Polyphosphoester in Crosslinked Copper Based Nanogels: Enhanced Antibacterial Performance Through Controlled Release of Copper," *Nanoscale* 9 (2017): 12664–12676, https://doi.org/10.1039/C7NR02446K.

55. M. Kim, Y. Kim, K. M. Lee, et al., "Electrochemical Improvement due to Alignment of Carbon Nanofibers Fabricated by Electrospinning as an Electrode for Supercapacitor," *Carbon* 99 (2016): 607–618, https://doi.org/10.1016/j.carbon.2015.12.068.

56. R. Sahay, V. Thavasi, and S. Ramakrishna, "Design Modifications in Electrospinning Setup for Advanced Applications," *Journal of Nanomaterials* 2011 (2011): 317673, https://doi.org/10.1155/2011/317673.

57. N. Bhardwaj and S. C. Kundu, "Electrospinning: A Fascinating Fiber Fabrication Technique," *Biotechnology Advances* 28 (2010): 325–347, https://doi.org/10.1016/J.BIOTECHADV.2010.01.004.

58. K. Garg and G. L. Bowlin, "Electrospinning Jets and Nanofibrous Structures," *Biomicrofluidics* 5 (2011): 13403, https://doi.org/10.1063/1.3567097.

59. A. Tariq, A. H. Behravesh, Utkarsh, and G. Rizvi, "Statistical Modeling and Optimization of Electrospinning for Improved Morphology and Enhanced β-Phase in Polyvinylidene Fluoride Nanofibers," *Polymers* 15 (2023): 4344, https://doi.org/10.3390/polym15224344.

60. A. K. Maurya, E. Mias, J. Schoeller, et al., "Understanding Multiscale Structure–Property Correlations in PVDF-HFP Electrospun Fiber Membranes by SAXS and WAXS," *Nanoscale Advances* 4 (2022): 491–501, https://doi.org/10.1039/D1NA00503K.

61. H. Na, Q. Li, H. Sun, C. Zhao, and X. Yuan, "Anisotropic Mechanical Properties of Hot-Pressed PVDF Membranes With Higher Fiber Alignments via Electrospinning," *Polymer Engineering & Science* 49 (2009): 1291–1298, https://doi.org/10.1002/pen.21368.

62. P. Kiselev and J. Rosell-Llompart, "Highly Aligned Electrospun Nanofibers by Elimination of the Whipping Motion," *Journal of Applied Polymer Science* 125 (2012): 2433–2441, https://doi.org/10.1002/app.36519.

63. M. D. Edwards, G. R. Mitchell, S. D. Mohan, and R. H. Olley, "Development of Orientation During Electrospinning of Fibres of Poly(ε-Caprolactone)," *European Polymer Journal* 46 (2010): 1175–1183, https://doi.org/10.1016/j.eurpolymj.2010.03.017.

64. A. M. El-hadi and F. Y. Al-Jabri, "Influence of Electrospinning Parameters on Fiber Diameter and Mechanical Properties of Poly(3-Hydroxybutyrate) (PHB) and Polyanilines (PANI) Blends," *Polymers* 8 (2016): 97, https://doi.org/10.3390/polym8030097.

65. A. R. Khodabandeh, A. A. Yousefi, and E. Vasheghani-Farahani, "The Effect of Process Variables on Near-Field Electrospinning of Polycaprolactone Studied by Response Surface Methodology," *Iranian Polymer Journal* 33 (2024): 1569–1581, https://doi.org/10.1007/s13726-024-01339-0.

66. S. Ma, T. Ye, T. Zhang, et al., "Highly Oriented Electrospun P(VDF-TrFE) Fibers via Mechanical Stretching for Wearable Motion Sensing," *Advanced Materials Technologies* 3 (2018): 1800033, https://doi.org/10.1002/admt.201800033.

67. A. Lafuma and D. Quéré, "Superhydrophobic States," *Nature Materials* 2 (2003): 457–460, https://doi.org/10.1038/nmat924.

68. M. Yao, Y. C. Woo, L. D. Tijing, et al., "Effect of Heat-Press Conditions on Electrospun Membranes for Desalination by Direct Contact Membrane Distillation," *Desalination* 378 (2016): 80–91, https://doi.org/10.1016/j.desal.2015.09.025.

69. R. Jiménez-Robles, B. M. Moreno-Torralbo, J. D. Badia, V. Martínez-Soria, and M. Izquierdo, "Flat PVDF Membrane With Enhanced Hydrophobicity Through Alkali Activation and Organofluorosilanisation for Dissolved Methane Recovery," *Membranes* 12, no. 4 (2022): 426, https://doi.org/10.3390/membranes12040426.

Supporting Information

Additional supporting information can be found online in the Supporting Information section.